ARTICLE

ECOSPHERE

Check for updates

Special Feature: Harnessing the NEON Data Revolution

Evaluation of vegetation indices and imaging spectroscopy to estimate foliar nitrogen across disparate biomes

Martha M. Farella^{1,2} | Mallory L. Barnes² | David D. Breshears^{1,3} | Jessica Mitchell⁴ | Willem J. D. van Leeuwen^{1,5} | Rachel E. Gallery^{1,3} |

¹School of Natural Resources and the Environment, Environment and Natural Resources 2, The University of Arizona, Tucson, Arizona, USA ²O'Neill School of Public and

Environmental Affairs, Indiana University, Bloomington, Indiana, USA ³Department of Ecology and Evolutionary

³Department of Ecology and Evolutionar Biology, The University of Arizona, Tucson, Arizona, USA

⁴Spatial Analysis Lab, University of Montana, Missoula, Montana, USA

⁵School of Geography, Development, and Environment, Environment and Natural Resources 2, The University of Arizona, Tucson, Arizona, USA

Correspondence

Martha M. Farella Email: farellam@iu.edu

Funding information

Arizona Agricultural Experiment Station, Grant/Award Number: AZRT-1390130-M12-222; National Science Foundation, Grant/Award Numbers: 1735693, 1916896

Handling Editor: R. Chelsea Nagy

Abstract

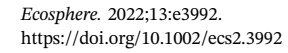
The nitrogen content in plant foliar tissues (foliar N) regulates photosynthetic capacity and has a major impact on global biogeochemical cycles. Despite its importance, a robust, time, and cost-effective methodology to estimate variation in foliar N concentration across globally represented terrestrial systems does not exist. Although advances in remote sensing data have enabled landscape-scale foliar N predictions, improved accuracy is needed to effectively capture variation in foliar N across ecosystems. Airborne remote sensing imagery was analyzed in conjunction with ground-sampled foliar chemistry data (n = 692), provided by the NEON, to predict foliar N at sites across the United States covering a variety of plant communities and climate types. We developed indices from novel two-band combinations that predicted foliar N more accurately than existing indices (≈8% improvement across all sites and a 45% improvement in arid sites). Compared with two-band indices, we increased accuracy and decreased bias of foliar N predictions by using full-spectrum reflectance information and partial least squares regression (PLSR) models ($R^2 = 0.638$; root mean square error = 0.440). Significant wavelengths included red edge (720-765 nm), near infrared (NIR) reflectance at 1125 nm, and shortwave infrared (SWIR) reflectance at 2050 and 2095 nm, which are regions indicative of foliar traits such as growth type (e.g., leaf area index with NIR) and photosynthetic parameters (e.g., chlorophyll and Rubisco with red and SWIR reflectance, respectively). With the confluence of rapid increases in computing power, several forthcoming or recently launched hyperspectral missions, and the development of large-scale environmental research observatories worldwide, we have an exciting opportunity to estimate foliar N across larger spatial areas covering more diverse biomes than ever before. We anticipate that these predictions will prove to be invaluable in helping to constrain biogeochemical model uncertainties across a global range of terrestrial ecosystems.

KEYWORDS

foliar nitrogen, hyperspectral, imaging spectroscopy, partial least squares regression, plant traits, remote sensing, Special Feature: Harnessing the NEON Data Revolution

This is an open access article under the terms of the Creative Commons Attribution License, which permits use, distribution and reproduction in any medium, provided the original work is properly cited.

© 2022 The Authors. Ecosphere published by Wiley Periodicals LLC on behalf of The Ecological Society of America.



INTRODUCTION

Photosynthesis is a primary control on net primary productivity (NPP) and determines rates of plant growth, food production, and ultimately carbon (C) uptake and storage, which has important implications for climate change. Since it is a major component of the essential photosynthetic machinery in leaves including lightharvesting compounds (chlorophyll) and proteins, the concentration of nitrogen in plant tissue (foliar N) controls these dynamics (Evans & Clarke, 2019; Field & Mooney, 1986). Foliar N is strongly correlated with photosynthetic capacity such that ecosystems with plants that have lower levels of foliar N can have a reduced C-uptake capacity (Field & Mooney, 1986). Nitrogen supply can significantly constrain plant productivity, with earth system model (ESM) simulations from 1850 to 2100 estimating up to a 61% reduction in net C uptake due to N limitation (Gastal & Saugier, 1989; Goll et al., 2012; Wang & Houlton, 2009; Wårlind et al., 2014). Notably, uncertainty in foliar N predictions across ecosystems in ESMs contributes to large variations in NPP predictions (Bonan et al., 2011; Friend, 2010; Rogers, 2014).

We currently lack a robust methodology to estimate variation in foliar N across terrestrial ecosystems. Estimates of foliar N concentrations typically involve in situ sampling followed by laboratory analysis of plant tissue using either the Dumas combustion or the Kjeldahl digestion techniques (Dumas, 1831; Horneck & Miller, 1997; Kjeldahl, 1883). Both of these techniques are time-intensive, and application of these methods across large spatial areas with an abundant and diverse community of plants is not typically feasible. Under controlled laboratory conditions, high spectral resolution data acquired from imaging spectrometers (hyperspectral data) can capture the narrowband absorption features leaf proteins exhibit and be used to predict foliar N content (Curran, 1989). At larger scales, remote sensing of hyperspectral data has advantages over traditional laboratory-based foliar N methods by capturing massive amounts of information regarding the plant N content of many different species across large areas and time frames. This methodology has been used to successfully model foliar N in a variety of systems (e.g., Chen et al., 2010; Clevers & Kooistra, 2012; Kalacska et al., 2015; Ollinger & Smith, 2005; Serrano et al., 2002; Skidmore et al., 2010). More challenging still is developing approaches to predicting foliar N that can be applied across diverse sites and biomes. Successful efforts include partial least squares regression (PLSR) approaches developed using sites in boreal forests (Ollinger et al., 2008), temperate and tropical forests (Martin et al., 2008), and temperature and sub-boreal forest ecosystems (Lepine et al., 2016; Singh et al., 2015). Recently, Wang et al. (2020)

successfully predicted foliar N from airborne hyperspectral data across eastern North American ecoregions (Wang et al., 2020). Arid systems are often excluded from crossbiome foliar N imaging spectroscopy studies (Lepine et al., 2016; Martin et al., 2008; Ollinger et al., 2008; Singh et al., 2015; Wang et al., 2020). Arid systems, defined as areas where total annual potential evapotranspiration greatly exceeds the average annual precipitation, cover 40% of the terrestrial land area and provide ecosystem services to more than 2 billion people (Millennium Ecosystem Assessment, 2005; UNEP-WCMC, 2011). They account for 30%-35% of terrestrial NPP and have large roles in both the trend and interannual variability in global carbon, water, and nitrogen cycles (Ahlstrom et al., 2015; Field, 1998; Poulter et al., 2014). The vegetation dynamics of arid systems such as patchiness, senescence, and rapid pulse-driven responsiveness to water availability cause many challenges in remote sensing analytics (Smith et al., 2019). Despite these obstacles, accurate retrieval of plant traits from remote sensing is possible and can provide valuable insight into changing plant dynamics in these arid systems (Eisfelder et al., 2012; Schmidt & Karnieli, 2000; Vicente-Serrano, 2007). Accurate cross-biome plant trait predictions from imaging spectroscopy require the inclusion of these arid systems in model building and validation.

Unfortunately, the availability of remotely sensed hyperspectral data is a major obstacle to achieving large-scale, cross-biome, foliar N mapping (Serbin & Townsend, 2020). Foliar N can exhibit high degrees of plasticity mediated by a variety of biotic and abiotic factors, which can add further complications to large-scale predictions (Abdala-Roberts et al., 2016; Chen et al., 2013; Osnas et al., 2018). For accurate predictions, the spatial resolution and spectral resolution of data need to capture subtle reflectance differences that result from variation both within and among species. Furthermore, consistent data collection from a variety of ecosystems is required for cross-biome comparisons. Neither requirement is trivial—imaging spectrometer sensors are costly, and acquisition of these data across space in a regular manner brings monetary, time, and logistical challenges. One emerging resource is the NEON, which is providing long-term open access data from ecological research sites across the United States. NEON is collecting both remote sensing and the plant chemistry data needed to estimate foliar N across broadscales (Johnson et al., 2010; Kampe, 2010).

Another popular approach in remote sensing is the use of vegetation indices to predict plant traits. Vegetation indices are designed to enhance spectral contribution from desired vegetation characteristics while minimizing the interference of other factors (Liang et al., 2012). Generally, vegetation indices are calculated from a discrete number of reflectance bands linked to a specific plant trait and are

ECOSPHERE 3 of 18

used to develop relationships between the trait of interest and reflectance properties of vegetation (Carlson & Ripley, 1997; Sims & Gamon, 2003). Two common vegetation indices, the Normalized Difference Vegetation Index (NDVI) and the Ratio Vegetation Index (RVI), have been repeatedly used in foliar N predictions (Lepine et al., 2016; van Deventer et al., 2015; Xue et al., 2004; Zhu et al., 2008). Both indices can be sensitive to soil brightness, however, especially when there is a small amount of vegetation cover. The Soil-Adjusted Vegetation Index (SAVI) can overcome this limitation and increase prediction performance by accounting for soil background effects (Huete, 1988). Many vegetation indices have also been developed to predict foliar N (Table 1). Most foliar N indices have been tested in specific systems—mainly the agriculture sector (Chen et al., 2010; Clevers & Kooistra, 2012; Reyniers et al., 2006; Tian et al., 2010; Wang, Yao, Tian, et al., 2012; Wang, Yao, Yao, et al., 2012; Xue et al., 2004; Zhu et al., 2008). As such, the applicability of these indices across diverse biomes has not been adequately evaluated.

In this study, we assessed the performance of published foliar N indices and the utility of imaging spectroscopy to estimate foliar N concentration across a range of ecosystems in the United States. Accurate plant trait predictions across broad spatial scales are needed to understand how plant community dynamics are responding to changing climate regimes. Our goal was to evaluate the ability of imaging

spectroscopy data to create generalizable predictions of variability in foliar N concentrations across ecosystems encompassing a range of climatic patterns and plant community types. We compared ground-sampled foliar N concentrations with high-resolution airborne imaging spectroscopy data and identified wavelength regions that related most strongly to foliar N concentration. Our analysis consisted of three components: First, the performance of previously published foliar N indices was evaluated across a diversity of sites; second, indices were calculated for all novel two-band combinations from NEON reflectance data and used to predict foliar N both within and across biomes; and last, the performance of these indices was compared with foliar N predictions using whole-spectrum statistical models to determine how the accuracy of predictions changed based on utilization of full-spectrum reflectance data and model complexity. We then highlight the implications of this improved approach for C-uptake modeling.

MATERIALS AND METHODS

Study sites, airborne imaging spectroscopy data, and foliar N

Foliar chemistry data (NEON, 2021a) were downloaded from the NEON data portal for all sites where foliar N

TABLE 1 Previously published foliar N vegetation indices included in analysis

Number	Citation	Vegetation index	Wavelengths included in vegetation index (nm)	System
1	Chen et al., 2010	Double-peak canopy nitrogen index (DCNI)	720, 700, 670	Agriculture
2	Clevers & Kooistra, 2012	Red-edge chlorophyll index $(CI_{red\ edge})$	780, 710	Grassland and agriculture
3	Lepine et al., 2016	Average NIR reflectance	800:850 and 800:1250	Temperate and boreal forests
3	Ollinger et al., 2008;	Average NIR reflectance	800:850 and 800:1250	Temperate and boreal forests
3	Wang et al., 2016	Average NIR reflectance	800:850 and 800:1250	Temperate forest
4	Reyniers et al., 2006	Optimal vegetation index (VI_{opt})	800, 670	Agriculture
5	Serrano et al., 2002	Normalized Difference Nitrogen Index (NDNI)	1510, 1680	Mediterranean
6	Tian et al., 2010	Blue N index	430, 495, 400	Agriculture
7	Wang, Yao, Yao, et al., 2012	Three broadband index	920, 700, 420	Agriculture
8	Wang, Yao, Tian, et al., 2012	SAVI (R_{822}, R_{738})	820, 735	Agriculture
8	Wang, Yao, Tian, et al., 2012	RVI (R_{822}, R_{738})	820, 735	Agriculture
9	Xue et al., 2004	RVI (R_{810}, R_{560})	810, 560	Agriculture
10	Zhu et al., 2008	RVI (R_{950}, R_{660})	950, 660	Agriculture
10	Zhu et al., 2008	RVI (R_{870}, R_{660})	870, 660	Agriculture
10	Zhu et al., 2008	RVI (R_{810}, R_{660})	810, 660	Agriculture

was sampled in conjunction with NEON's Airborne Observation Platform campaign from 2017 to 2019 (N = 692) (Figure 1, Appendix S1: Tables S1 and S2) using the neonUtilities package in R version 4.0.2 (Lunch et al., 2021; R Core Team, 2021). Full details regarding NEON protocols for canopy foliage sampling can be found in NEON.DOC.001024 revisions D and E (for 2017-2018 sites) and revision F (2019 sites; Weintraub & Hinckley, 2017). Briefly, the majority of plant samples included in the present analysis were collected from a subset of the "Distributed Base Plots" (40 × 40 m) and "Tower Plots" (sizes differ by location) for a total of 14-20 plots per site. When there was more than 25% aerially visible woody species in a plot, a maximum of the top three most abundant species were identified and fully sun-lit vegetation from a single individual of each of these species was sampled. When there was less than 25% of aerially visible woody species or more than 25% aerially visible nonwoody herbaceous species, herbaceous clip strips were also collected from plots. Herbaceous clip strips were representative of the herbaceous plant biomass and randomly collected from a 0.1×2 -m area of sun-lit vegetation (not located under overstory canopy) in the plot area and homogenized. Plant sample locations were determined with the geoNEON R package (NEON, 2020). A threshold of 85% cover was applied to the herbaceous clip strips to ensure inclusion of samples with sufficient foliar coverage over an area captured by a single pixel of the remote sensing data while excluding nonfoliated areas (Asner et al., 2015). Woody plant sample locations were determined based on vegetation structure data (NEON, 2021b; Appendix S1: Table S1).

Biome delineations for sample locations were determined from the Köppen-Geiger climate classifications defined in Kottek et al. (2006) using the downscaling algorithms defined in Rubel et al. (2017) (Figure 1). We chose this biome classification scheme because it predicts biome distributions based on monthly and annual patterns in temperature and precipitation while considering plant threshold values to these trends; it has been widely used in ecological modeling and climate change research (Franks et al., 2018; Köppen, 2011; Mahlstein et al., 2013; Poulter et al., 2011). Delineating sites according to biome allowed us to produce generalizable prediction models where sites were grouped according to similar vegetation types, cover, and climatic conditions (Appendix S1: Table S2). When available, high-resolution red, green, and blue imagery for each site was used to calculate the Green Leaf Index (GLI) of sample locations (NEON, 2021c). Values for GLI range from -1 to +1 with negative values indicating soil and nonliving vegetation and positive values indicating green vegetation (Louhaichi et al., 2001). Leaf Area Index (LAI) was calculated from the hyperspectral

imagery for the sample locations using the equation outlined in NEON protocols (Hulslander, 2019). Additional meta-data for each site including sample type and number, National Land Cover Database classification, dates samples were collected, location, GLI, and LAI are included in Appendix S1: Table S2.

NEON's imaging spectrometer measures spectral radiance in 426 channels across a wavelength range of 385–2510 nm in 5-nm increments at 1-m² spatial resolution. The orthorectified surface reflectance data product from individual flight lines was used in the analysis (NEON, 2021d; Appendix S1: Table S1). This data product is calibrated and atmospherically corrected (ATCOR) with ATCOR reflectance processing. Whenever possible, data products were selected from low cloud cover (<10%) conditions. Corrections for topographic illumination effects were performed using the modified sun-canopy sensor topographic method (Soenen et al., 2005).

To normalize between and within scenes for differential illumination and reflectance due to sun-target-sensor geometry, we performed a bidirectional reflectance distribution function (BRDF). For both topographic and BRDF corrections, we modified code from the openly available python package HyTools (Chlus et al., 2019) to work directly on .h5 files (Farella, 2021), which is the native format of NEON hyperspectral reflectance data. We used semi-empirical radiative transfer approximations to derive our kernel-based BRDF correction model (Colgan et al., 2012; Hilker, 2018; Wanner et al., 1995; Weyermann et al., 2015). Similar to the BRDF model developed for Moderate Resolution Imaging Spectrometer reflectance and albedo data products, we determined reflectance with the Li-sparse model to compute the geometric scattering kernel and the Ross-thick model to compute the volumetric scattering kernel as functions of viewing and illumination geometry (Li & Strahler, 1992; Los et al., 2005; Ross, 1981; Schaaf et al., 2002). Li kernel canopy parameters were fixed according to Colgan et al. (2012) as 2.0 and 10.0 for object shape (h/b) and height (b/r), respectively. Correction factors for reflectance anisotropy at each reflectance band were calculated as a function of the modeled reflectance at the actual view angle and the modeled reflectance at nadir (Weyermann et al., 2015). The prevalent solar zenith angle at the time of data acquisition was between 35° and 40° with $\approx 90\%$ of the flight lines having solar zenith angles <45°.

Reflectance spectra were extracted from a 3-m area centered on the plant clip location to account for geolocation errors. These nine reflectance readings were then averaged to a single reflectance reading for each plant clip. The GLI and LAI for this area were calculated to ensure reflectance represented live vegetation and did not consist primarily of nonliving plant and soil reflectance.

ECOSPHERE 5 of 18

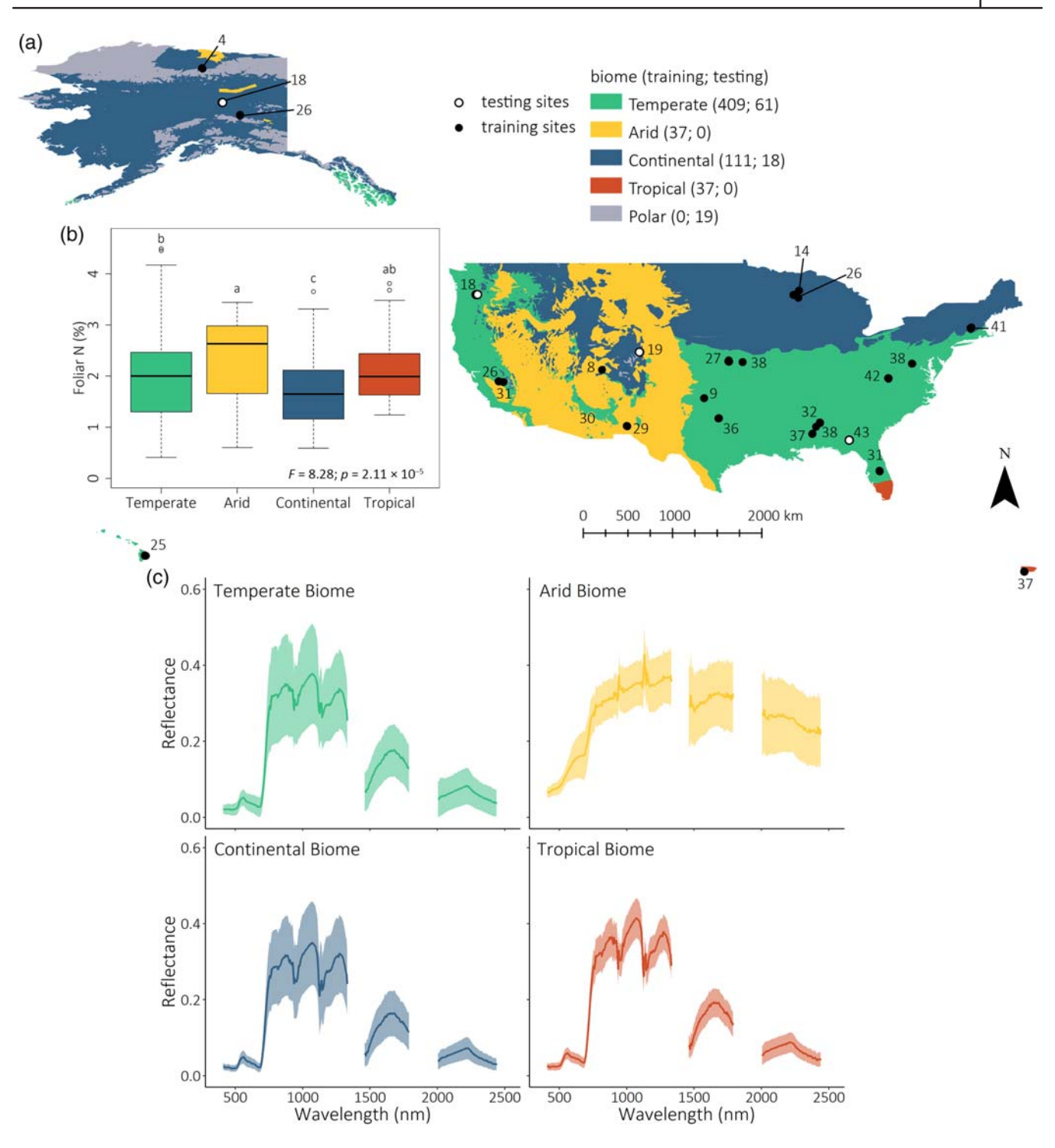


FIGURE 1 Map of sample locations across the United States and Puerto Rico symbolized according to biomes (a). Numbers on map represent the number of samples at each site. Boxplot shows median foliar nitrogen (N) percent distribution for each biome with ANOVA and Tukey's honestly significant difference post hoc analysis results (b). Outliers are symbolized as open points, and whiskers extend to lower and upper quartiles 1.5 times the interquartile range. Individual graphs for each biome display the average (line) and standard deviation (shaded region) spectral reflectance values across wavelengths (c)

Distance between sample locations was determined with Euclidean distance with less than 0.2% of samples included in the analysis being closer than 3 m to other samples (Appendix S1: Table S2), ensuring unique

reflectance spectra from each sample for comparison with measured foliar N.

Three different sensors were used to collect the hyperspectral data across the NEON sites included in

this analysis, and band centers between the sites did not always align due to shifts that can occur during the sensor calibration process (Green et al., 1998). As such, we resampled reflectance readings from 385 to 2510 in 5-nm increments to ensure all reflectance spectra could be analyzed together. Prior to analysis, reflectance spectra were trimmed at the far ends of the spectrum and noisy regions dominated by water absorption leaving 340 of the 426 bands of reflectance data over the 385–2510-nm region. The resulting reflectance bands used in the analyses spanned the wavelengths: 410–1330 nm, 1460–1790 nm, and 2005–2440 nm (Figure 1).

Foliar nitrogen indices and analyses

Many vegetation indices have been developed to predict foliar N concentration. Fourteen previously published indices that specifically measure foliar N (in contrast to vegetation indices that measure chlorophyll or photosynthesis as proxies for foliar N) were selected for comparative analysis in this study (Table 1).

We also calculated foliar nitrogen indices (FNI) with three commonly used vegetation index calculations (Equations 1–3) using all two-band combinations of reflectance data. Combinations of the 340 bands included in the data analyses according to Equations (1)–(3) resulted in 115,260 unique band combinations. Analysis was done across all sites and on data subdivided by biome. The optimum FNI was chosen as the two-band combination that had the highest average R^2 as long as the average root mean square error of prediction (RMSEP) values across biomes fell within the lowest 25% (first quartile) of values.

$$FNI_{NDVI} = \frac{R_{band1} - R_{band2}}{R_{band1} + R_{band2}}$$
 (1)

$$FNI_{SAVI} = \frac{1.5(R_{band1} - R_{band2})}{0.5 + R_{band1} + R_{band2}}$$
(2)

$$FNI_{RVI} = \frac{R_{band1}}{R_{band2}}$$
 (3)

where R is the reflectance value from a single band of data.

In addition to two-band indices, PLSR models were run on full-spectrum reflectance and all FNI two-band combinations. We performed 100 permutations of the data with 80% of the data used for model training and 20% used for model testing. Models were validated using 10-fold cross-validation. To avoid model overfitting, the

number of components for each model was chosen as the minimum RMSEP for up to 20 components. The models that had the best performance for foliar N predictions with the testing data (test R^2 > average test R^2 for the 100 iterations and test RMSEP < average test RMSEP) were used to calculate coefficient values and generate model statistics such as R^2 , RMSE, and variable importance in projection (VIP) scores (Chadwick & Asner, 2016). To improve spectra consistency, crossspectrum brightness normalization was applied to reflectance spectra before running the single-band PLSR models. Brightness normalization helps minimize differences among spectra due to variations in structure, viewing angle, and LAI (Feilhauer et al., 2010). To accurately evaluate model performance, PLSR coefficients were applied to four novel sites (BONA, JERC, NIWO, and WREF) completely excluded from model building. PLSR was implemented using the pls package in R (Mevik et al., 2020). VIP scores were calculated with the plsVarSel R package (Mehmood et al., 2012).

Heat graphs of R^2 linear regressions and PLSR VIP scores were used to illustrate the importance of two-band combinations as predictors of foliar N from hyperspectral data using the gplots R package (Warnes et al., 2020). Maps were created in ArcGIS Pro version 2.4.1.

RESULTS

There was variation in both reflectance spectra and foliar N concentration among the biomes included in the analysis (Figure 1). Samples from sites in the arid biome had the highest foliar N values ($\overline{x}=2.33\%$), while continental biome sites had the lowest ($\overline{x}=1.68\%$). In total, 594 samples were included in model building and 98 samples were included in model testing from sites across the United States with most of the samples coming from temperate biomes (N=470) and the least coming from arid and tropical biomes (N=37 from each biome; Figure 1).

When samples across biomes were pooled, all 14 previously published foliar N indices captured less than 18% of the variation in foliar N (Table 2, Figure 2). The best index across all sites was the SAVI foliar N index published in Wang, Yao, Tian, et al. (2012) using reflectance at 820 and 735 nm ($R^2=0.178$). Considering individual biomes, the SAVI foliar N index also had the highest performance in the temperate biome ($R^2=0.294$). In the arid biome, the Normalized Difference Nitrogen Index using reflectance at 1510 and 1680 nm had the best performance ($R^2=0.130$). The RVI using reflectance at 950 and 660 nm performed best in the continental biome ($R^2=0.203$). Across the board, foliar N indices

ECOSPHERE 7 of 18

in tropical biomes performed poorly—there was a maximum of 16.7% of the variance explained in foliar N by the double-peak canopy N index using reflectance at 670, 700, and 720 nm.

Compared with previously published indices, the FNI calculations evaluated in this study had improved performance metrics. The optimum two-band calculation for all three indices showed modest improvement across all sites pooled (~8% increase), with a large improvement in sites from arid biomes (R^2 increased from 0.130 to 0.586; Table 3, Figure 2). For all three FNI calculations, the optimum two-band combination used bands from the SWIR around 2050 nm and 2100 nm and explained over 20% of the variance in foliar N when all sites were pooled. Sites in arid biomes had over 50% of the variance in foliar N explained by optimum two-band indices with all three FNI calculations. The FNI_{NDVI} and FNI_{RVI} calculations also performed well in sites from temperate biomes with ~40% of the variance in foliar N explained. The FNI_{SAVI} calculation had the best performance in sites from the continental biome (Table 3). Again, indices did not perform as well in sites from the tropical biome, with a maximum of 1.2% of the variance in foliar N explained by the ${\rm FNI}_{\rm NDVI}$ calculation.

Considering all two-band combinations, rather than just the optimum two-band FNI calculations, heat graphs illustrate correlations between foliar N and the FNI calculations for each of the 115,260 two-band combinations (Figure 3, Appendix S1: Figures S1 and S2). Similar FNI regions performed well across biomes: 600–700 nm with both 1500–1750 and 2100–2300 nm; 2020–2050 nm with 2075–2320 nm. There was also a small interval at 710–720 nm with 800–1250 nm, especially considering the tropical biome. Overall, the highest R^2 values were seen in sites from temperate, arid, and continental biomes. The tropical biome had a maximum of 31.1% of the variance explained in foliar N with the FNI_{NDVI} calculation using a visible light reflectance band combination (755 and 765 nm).

Utilizing the full-spectrum reflectance in PLSR analysis led to further improvements in model performance (Table 3). When all sites were pooled together, 63.8% of

TABLE 2 Comparison of previously published foliar N index performance (R^2) by biome

Citation	Formula	All sites	Temperate	Arid	Continental	Tropical
1	$\frac{(R_{720} - R_{700})}{(R_{700} - R_{670})} / (R_{720} - R_{670} + 0.03)$	0.005*	0.012*	0.000	0.012	0.167**
2	$\left(\frac{R_{780}}{R_{710}}\right)-1$	0.125**	0.246**	0.003	0.011	0.095*
3	$rac{1}{11}\sum_{i=800}^{850}R_i$	0.152**	0.181**	0.084*	0.116**	0.000
3	$\frac{1}{91} \sum_{i=800}^{1250} R_i$	0.132**	0.134**	0.049	0.144**	0.000
4	$\frac{1.45 \times (R_{800}^2 + 1)}{R_{670} + 0.45}$	0.095**	0.231**	0.000	0.100**	0.000
5	$\frac{\log\left(\frac{1}{R_{1510}}\right) - \log\left(\frac{1}{R_{1680}}\right)}{\log\left(\frac{1}{R_{1510}}\right) + \log\left(\frac{1}{R_{1680}}\right)}$	0.119**	0.289**	0.130*	0.196**	0.000
6	$rac{R_{430}}{R_{495} imes R_{400}}$	0.005*	0.003	0.059	0.117**	0.000
7	$\frac{R_{920} - R_{700} + 2 \times R_{420}}{R_{920} + R_{700} - 2 \times R_{420}}$	0.006*	0.057**	0.000	0.000	0.000
8	$\frac{1.5(R_{820} - R_{735})}{R_{820} + R_{735} + 0.5}$	0.178**	0.294**	0.000	0.187**	0.066
8	$rac{R_{820}}{R_{735}}$	0.091**	0.191**	0.000	0.036*	0.140*
9	$\frac{R_{810}}{R_{560}}$	0.140**	0.260**	0.091*	0.111**	0.031
10	$\frac{R_{950}}{R_{660}}$	0.008*	0.012*	0.000	0.203***	0.054
10	$rac{R_{870}}{R_{660}}$	0.045	0.012*	0.000	0.079**	0.045
10	$\frac{R_{810}}{R_{660}}$	0.009*	0.013*	0.000	0.087**	0.050

Note: Asterisks (* and **) indicate significance (p < 0.05 and 0.01). "R" in the formula column refers to reflectance at the wavelength identified as a subscript. Citations refer to the citation numbers listed in Table 1.

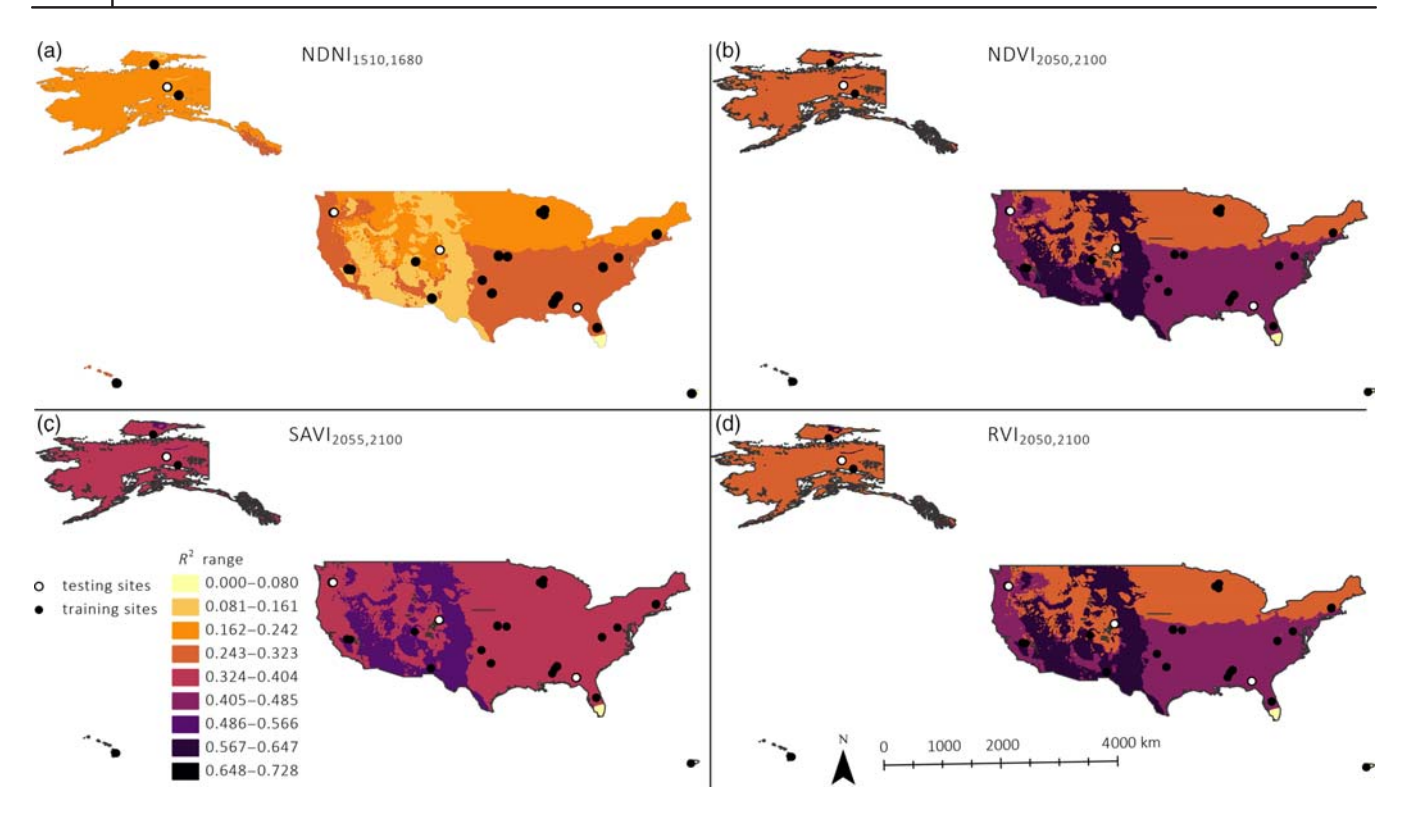


FIGURE 2 Comparison of foliar nitrogen index (FNI) performance (R^2) by biome. Darker and lighter colors indicate FNI that had better and worse (respectively) predictive power. (a) Performance of the Normalized Difference Nitrogen Index (NDNI) published in Serrano et al. (2002) and (b–d) the best-performing two-band indices analyzed in the present analysis according to the Normalized Difference Vegetation Index (NDVI)-style calculation (b), Soil-Adjusted Vegetation Index (SAVI)-style calculation (d)

TABLE 3 Comparison of foliar N index performance (R^2 and root mean square error [RMSE]) by biome

	All sites		Temperate		Arid		Continental		Tropical	
Model	R^2	RMSE	R^2	RMSE	R^2	RMSE	R^2	RMSE	R^2	RMSE
$FNI_{NDVI} = \frac{R_{2050} - R_{2100}}{R_{2050} + R_{2100}}$	0.260	0.653	0.409	0.580	0.586	0.530	0.301	0.581	0.012	0.665
$FNI_{SAVI} = \frac{1.5(R_{2055} - R_{2100})}{0.5 + R_{2055} + R_{2100}}$	0.239	0.662	0.361	0.603	0.516	0.573	0.338	0.566	0.006	0.668
$FNI_{RVI} = \frac{R_{2050}}{R_{2100}}$	0.261	0.652	0.411	0.579	0.585	0.530	0.303	0.581	0.011	0.666
PLSR ₄₂₆	0.638	0.440	0.625	0.433	0.697	0.474	0.695	0.391	0.316	0.610
$PLSR_{NDVI}$	0.636	0.456	0.617	0.457	0.725	0.512	0.664	0.420	0.235	0.615
PLSR _{SAVI}	0.656	0.434	0.667	0.430	0.725	0.459	0.708	0.389	0.258	0.942
PLSR _{RVI}	0.240	0.663	0.363	0.601	0.619	0.554	0.506	0.521	0.240	0.689

Note: Foliar nitrogen index (FNI) reflectance (*R*) wavelengths represent the best two-band combination for each calculation. Partial least squares regression (PLSR) results are presented for the single bands (PLSR₄₂₆) and two-band calculations (PLSR_{NDVI}, PLSR_{SAVI}, and PLSR_{RVI}).

the variance in foliar N was explained by the PLSR model using all reflectance bands. The best single-band PLSR performance occurred in sites from arid and continental biomes where over 69% of the variance in foliar N was explained by the PLSR models. The tropical biome had 31.6% of the variance in foliar N explained by the PLSR using individual reflectance bands. Similar regions of the

spectrum emerged as having strong predictive power for foliar N both within and among biomes (Figure 4). Consistently, reflectance at 2005, 1125, 940, 765, and 720 nm had high VIP scores. In the arid biome, reflectance from 1475 nm also scored highly. In the temperate biome, reflectance around 765 nm was also an important predictor of foliar N.

ECOSPHERE 9 of 18

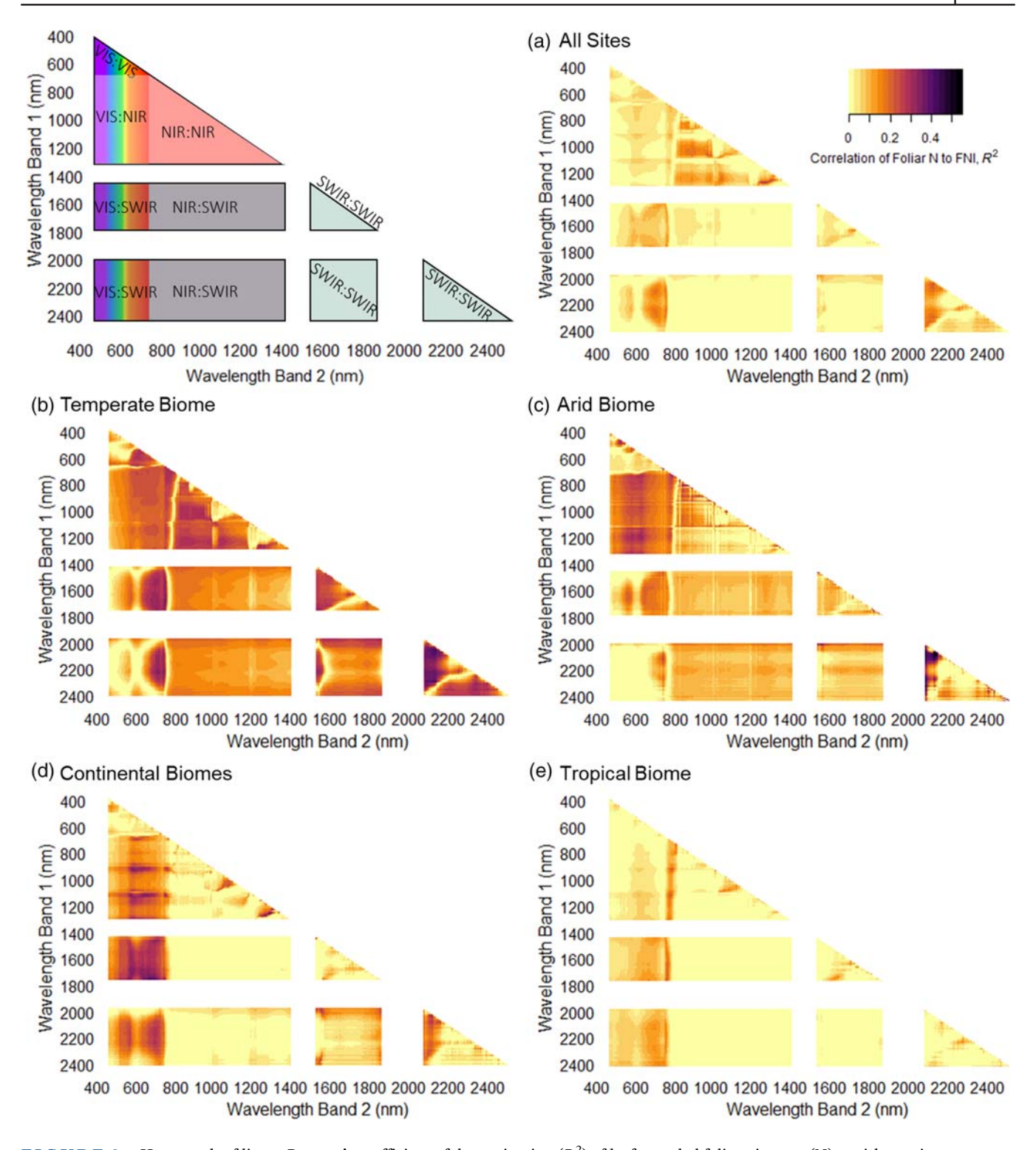


FIGURE 3 Heat graph of linear Pearson's coefficient of determination (R^2) of leaf-sampled foliar nitrogen (N) to airborne imagery spectra between all combinations of two bands with the Normalized Difference Vegetation Index calculation for all sites (a), and sites in the temperate (b), arid (c), continental (d), and tropical (e) biomes. Strong (dark purple) and weak (light orange) coefficients exist in several broad spectral regions. Figure in the top left corner is a conceptual diagram illustrating the location of band combination regions on the heat graph area

Considering PLSR models run on FNI two-band combinations, there was a slight improvement in foliar N predictions for the FNI_{SAVI} but not for FIN_{NDVI} or FNI_{RVI}

calculations across all sites (Table 3). In addition to the best performance when all sites were pooled, FNI_{SAVI} also had the best performance in all individual biomes (Table 3).

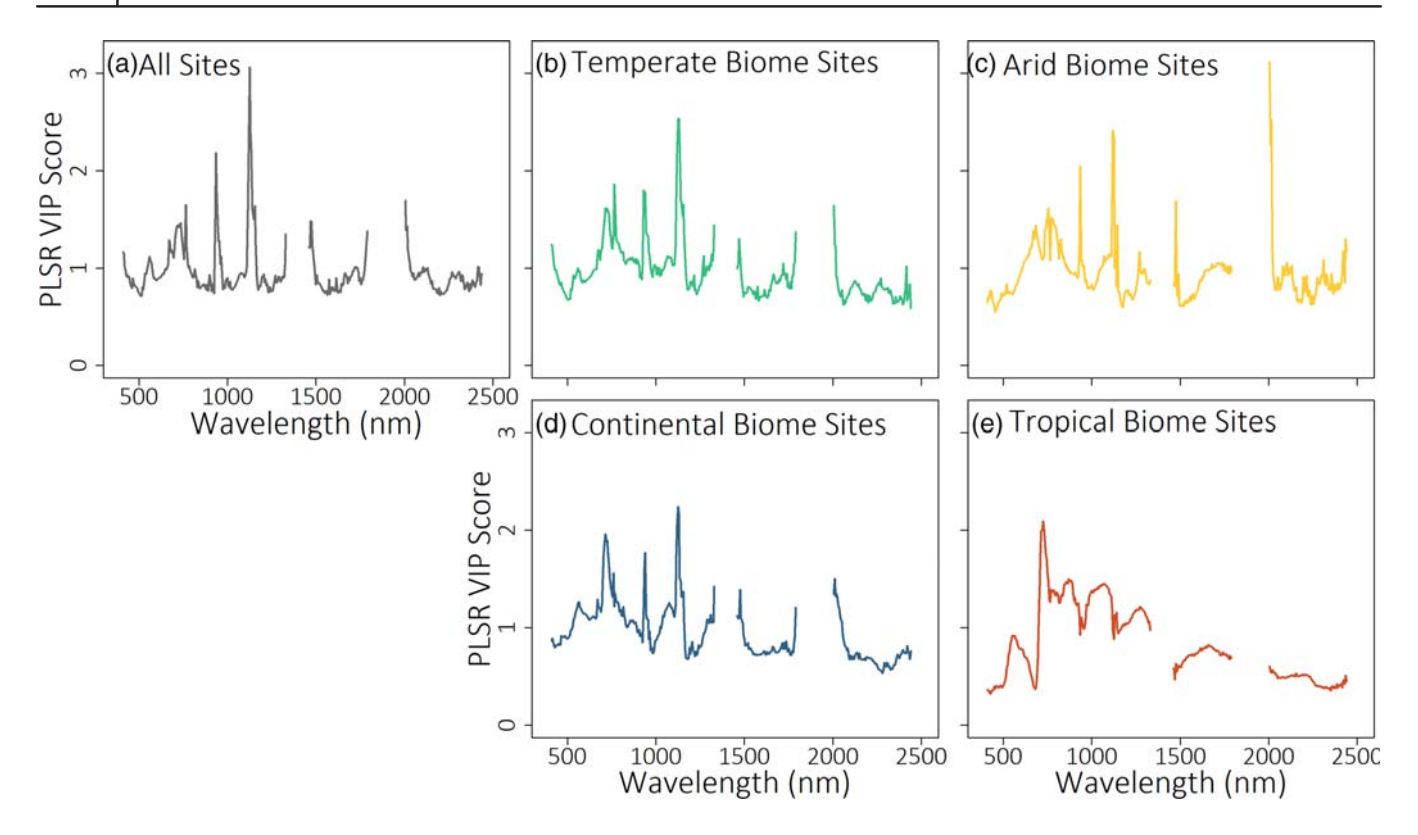


FIGURE 4 Partial least squares regression (PLSR) variable importance in the projection (VIP) scores for all spectral wavelengths from models predicting foliar nitrogen (N) as a function of reflectance for all sites (a), temperate (b), arid (c), continental (d), and tropical (e) biomes. Values plotted are mean VIP scores based on the models from 100 permutations where test root mean square error (RMSE) < average test RMSE and test R^2 > average test R^2

There were band combinations throughout the spectrum that were important in explaining the variance in foliar N (Figure 5, Appendix S1: Figures S3 and S4). Across all biomes, the visible portion of the spectrum (410-710 nm) in combination with parts of the SWIR portion of the spectrum (2005-2440 nm) was an important region in the FNI_{NDVI} PLSR models. In the temperate and continental biomes, band combination regions from the visible portion of the spectrum (410-550 nm with 440-725 nm) were also important regions in the FNI_{NDVI} and FNI_{SAVI} PLSR models (Figure 5, Appendix S1: Figure S3). In the continental and tropical biomes, wavelengths centered around 1460 nm combined with reflectance throughout the visible spectrum (380-750 nm) were important in the FNI_{NDVI} PLSR model. The tropical biome NIR and SWIR band combinations were important predictors of foliar N in the FNI_{SAVI} PLSR model (Appendix S1: Figure S3). In the FNI_{RVI} PLSR models, visible light combinations with NIR reflectance were important predictors of foliar N (Appendix S1: Figure S4).

Single-band and ${\rm FNI_{NDVI}}$ PLSR models tested on four sites excluded from model building have variable performance (Figure 6). The two PLSR models performed poorly in sites from continental biomes with less than

20% of the variance in foliar N predicted. Sites from polar biomes, which were biomes completely excluded from model building, had 26% and 40% of the variance in foliar N predicted by the single-band and FNI_{NDVI} PLSR models, respectively. PLSR models captured over a third of the variance in foliar N at sites in temperate biomes (Figure 6). Overall, the two-band PLSR model performed better than the single-band model for all testing sites evaluated (R^2 for all testing samples combined = 0.168 and 0.236 for single-band and FNI_{NDVI} PLSR models, respectively).

DISCUSSION

Collectively, these results show the utility of a single statistical model built on imaging spectroscopy data at capturing spatial variation in foliar N concentration across a range of ecosystems in the United States Both fine spatial resolution data and narrowband reflectance patterns across the spectrum (visible, NIR, and SWIR) were important in accurately capturing the subtle differences in foliar N concentrations. Specifically, SWIR wavelength regions previously shown to correspond to high N concentration plant tissue continually

ECOSPHERE 11 of 18

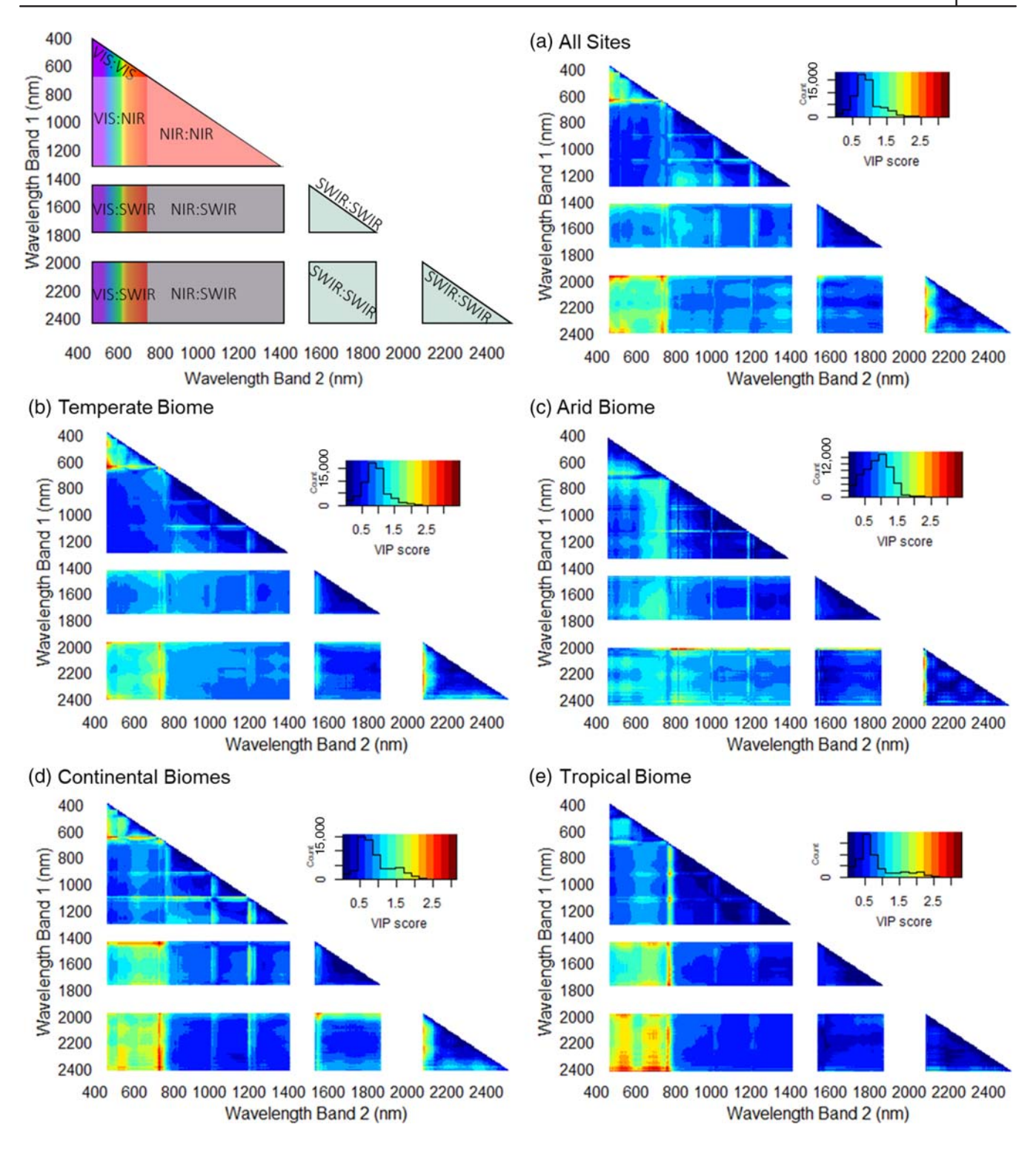


FIGURE 5 Variable importance scores for all spectral wavelengths from partial least squares regression (PLSR) models predicting foliar nitrogen (N) as a function of foliar nitrogen index (FNI) two-band combinations using the Normalized Difference Vegetation Index (NDVI)-style foliar N calculation for all sites for all sites (a), and sites in the temperate (b), arid (c), continental (d), and tropical (e) biomes. Values plotted are mean variable importance in the projection (VIP) scores based on the models from 100 permutations where test root mean square error (RMSE) < average test RMSE and test R^2 > average test R^2 . Darker red colors indicate regions that are more important in relation to the explanation of foliar N variance. Figure in the top left corner is a conceptual diagram illustrating locations of band combination regions on the heat graph area

emerged as an important predictor of foliar N across biomes. Our analysis moves beyond past foliar N predictions from imaging spectroscopy by investigating unique two-band indices and by including sites from arid biomes. Our results have broad implications for ESMs and provide insight into future spaceborne missions.

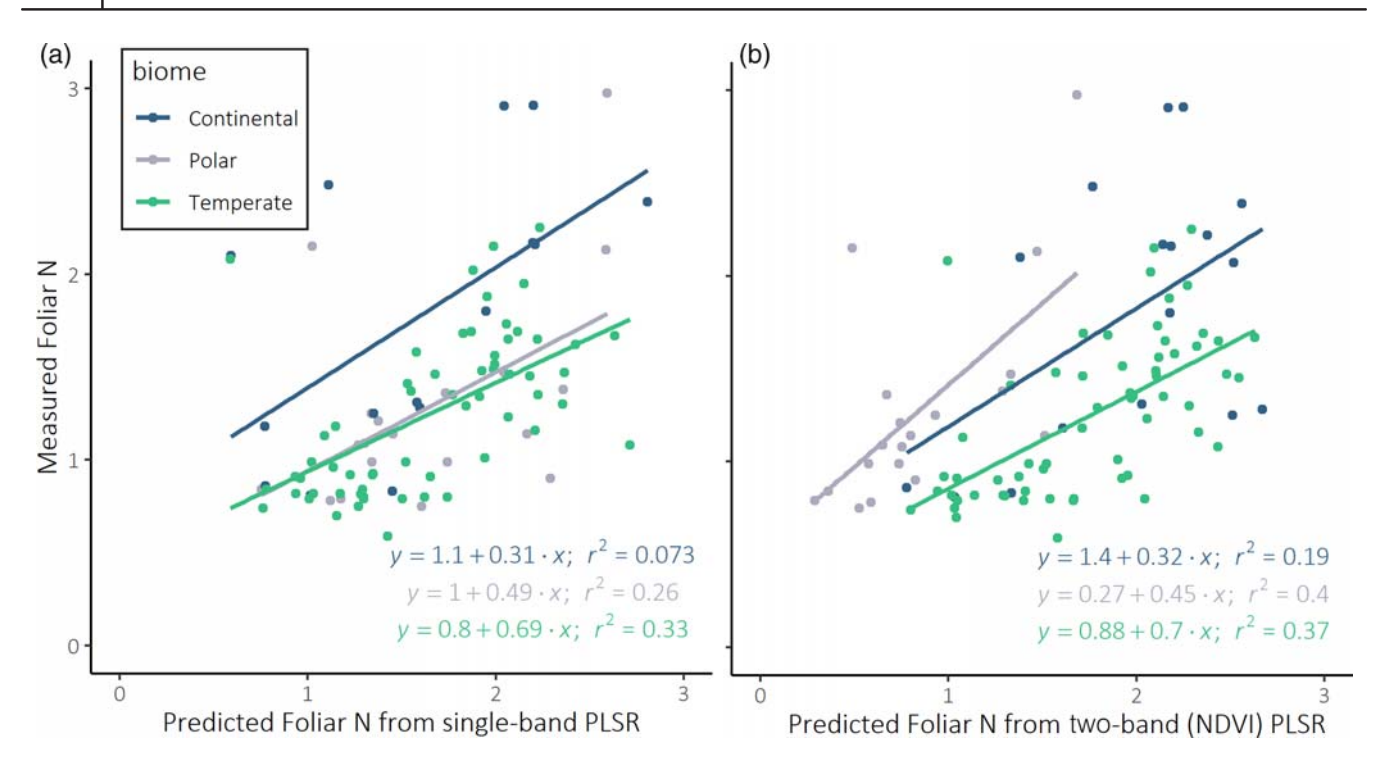


FIGURE 6 Evaluation of model performance at testing sites. Single-band (a) and foliar nitrogen index (FNI) two-band combinations using the Normalized Difference Vegetation Index (NDVI) calculation and (b) partial least squares regression (PLSR) model predictions (*x*-axis) compared with measured values (*y*-axis) for the four sites excluded from model building. Sites are symbolized according to biome classifications. Linear equations and R^2 values for each biome are provided in the lower right-hand corner of each graph

Enhanced foliar N predictions (PLSR model)

Models linking spectral signatures to plant traits are frequently built at a single location or point in time and, subsequently, may not effectively capture variation in plant reflectance patterns that result from differences in plant type, vegetation structure, or phenology (Gamon et al., 2019; Serbin & Townsend, 2020). As such, the suitability of these context-specific empirical models should not be assumed without first testing their applicability (Ustin & Jacquemoud, 2020), and often, models display reduced performance metric when applied to novel datasets (Glenn et al., 2008; Lepine et al., 2016; Wang et al., 2016). For plant trait models to provide accurate predictions on novel datasets and systems, they need to be developed on a wide range of variability in plant characteristics. Due in part to the difficulty of obtaining coordinated foliar N samples across biomes, most studies evaluate a specific plant community (e.g., forests; Lepine et al., 2016; Martin et al., 2008; Singh et al., 2015). Wang et al. (2020) leveraged NEON data to successfully predict foliar N from airborne hyperspectral imagery across eastern US ecoregions. Our study is the first to predict foliar N in western US ecoregions, including arid biomes. Given the coverage and importance of arid biomes in

global biogeochemical models, accurate representation of these systems in cross-biome analyses is necessary. The datasets provided by NEON covering a variety of sites, edaphic characteristics, climate patterns, plant traits, and community dynamics offered us and continue to offer a unique opportunity for the potential development of empirical models that are relevant across broad environmental contexts.

When analysis was not limited to only two discrete reflectance values (through the calculation of vegetation indices) but all wavelength regions across the spectrum were used to predict foliar N, the strongest results were seen both within and across biomes (Tables 2 and 3). Our results across diverse plant communities and biomes (including arid sites) are comparable to other studies that have used imaging spectroscopy with PLSR for foliar N predictions (Lepine et al., 2016, Martin et al., 2008, Singh et al., 2015). Correlations between foliar N and indices showed that both narrowband and broadband regions were strong predictors of foliar N. Furthermore, these regions varied depending on the biome analyzed (Figures 3-5). As such, the PLSR approach using the complete spectrum produced the best results because it was able to leverage important regions across the spectrum and discern differences in foliar N both between and within varying biomes. The full-spectrum PLSR can

ECOSPHERE 13 of 18

capture both the direct effects of foliar N on plant spectra and the indirect effects of foliar N on various associations that impact light scattering and reflectance such as plant structural features and C assimilation (Lepine et al., 2016).

Significant wavelength regions in our PLSR coincide with regions that have been identified in past studies. For example, the red edge contains strong chlorophyll absorption and canopy scattering patterns making it a useful region for predictions of chlorophyll and foliar N content (Cho & Skidmore, 2006; Clevers & Gitelson, 2013; Mutanga & Skidmore, 2007; Ramoelo et al., 2012; Smith et al., 2003). Similarly, we found reflectance patterns in the red edge to be important constituents in PLSR models both within and across biomes with VIP values peaking at bands centered on 720 and 765 nm (Figure 4). Given the importance of these regions, first derivatives of the red and NIR edges might be useful for cross-biome foliar N predictions, though evaluation of these calculations across space and time is required (Cho & Skidmore, 2006; Mutanga & Skidmore, 2007). Other important regions in the VIP graphs occurred in the NIR region (930-965 and 1110-1160 nm). The NIR region can contain spectral variation due to structural variables that covary with foliar N concentrations and can influence overall reflectance and absorption from this region (Figure 4; Knyazikhin et al., 2013; Lepine et al., 2016; Ollinger, 2011; Ollinger et al., 2008). Although narrowbands within the NIR region continually emerged as important predictors of foliar N (Figures 3–5), averaged reflectance values over this whole region did not explain more than 20% of the variance in foliar N (Table 2). Since only specific portions of the NIR were important, this might be due to atmospheric effects rather than broad structural changes with changing N concentrations. Together, results suggest that PLSR models, which leverage reflectance patterns from both the NIR and alternate portions of the spectrum, can capture the direct and indirect effects of foliar N reflectance, absorption, and light scattering patterns across disparate sites and biomes.

Past and present foliar N indices

Past indices evaluated in this study consistently predicted less than 30% of the variance in foliar N on individual biomes and less than 15% of the variance in foliar N when sites from all biomes were pooled together (Table 2, Figure 2). Vegetation indices reduce the total amount of reflectance information obtained from a remote sensing platform into a smaller number of optical properties that are highly correlated with the trait of interest. When this simplification occurs, portions of the spectrum containing information relevant to the trait of interest may be excluded from the final index calculation. For example, 23 separate absorption features spanning

visible, NIR, and SWIR regions are associated with compounds that influence plant N content (Curran, 1989; Elvidge, 1990) and it would be impractical to include information from all these regions into a single vegetation index calculation for foliar N. Even so, it is possible to identify regions in reflectance spectra that help explain significant proportions of variance in the desired trait of interest.

The indices evaluated in this present study outperformed previously published vegetation indices. All three best FNI calculations included reflectance around 2050 and 2100 nm (Table 3, Figure 2). Laboratorycontrolled experiments on dried foliage have shown both of these SWIR regions to be associated with foliar N dynamics with D-ribulose 1,5-diphosphate carboxylase (Rubisco) having strong absorption at 2050 nm and cellulose, lignin, hemicellulose, and starch compounds having absorption features at 2095 nm (Elvidge, 1990). Rubisco, the enzyme needed for the first step of photosynthesis, requires a significant amount of N and typically makes up about 25% of the total N in photosynthetic cells (Chapin et al., 2011). Despite these findings, further analysis is needed to determine whether airborne imaging spectroscopy is directly sensing N-rich cellular components or indirectly picking up foliar N absorption patterns caused by variation in plant structural traits that relate to adaptive strategies intended to optimize light harvesting such as leaf area density and LAI (Knyazikhin et al., 2013; Lepine et al., 2016; Ollinger, 2011; Ollinger et al., 2008). Regardless, these findings suggest a crosssite vegetation index can accurately capture variation in plant N concentration based on narrowband reflectance differences due to potential variations in plant traits that relate to the concentration of N-rich compounds within plant tissues.

The indices did not perform as well in sites from the tropical biome compared with other biomes. The sample size was smaller (n = 37) in the tropics than in many of the other biomes, which possibly explains a portion of the poor performance from these sites. Additively, none of the published indices analyzed in the present study were developed in tropical regions; they were mostly developed in agriculture systems with some developed in grasslands or temperate forests (Table 1). Plant structure, which is generally more complex in tropical regions than these other systems, may saturate the reflectance pattern from N in these systems (Knyazikhin et al., 2013). It is also worth noting that all of the tropical samples in this analysis came from Puerto Rico in April 2018. This was only 7 months after Hurricane Maria, which devastated the island and could have impacted foliar N concentration and spectral reflectance patterns. NDVI, however, returned to normal just 1.5 months after the hurricane,

so it is more likely that the complex vegetation structure, vegetation diversity, and low sample size are the possible explanations for poor performance from these sites (Hu & Smith, 2018).

When scaling up leaf traits such as foliar N, it is important to consider that for an area at any given time, top of canopy reflectance values represents not only reflectance from the plant of interest but also reflectance from a mixture of other plants, soil, and background reflectance. Together, these confounding influences can combine through complex light interactions including nonlinear scattering. In a semiarid system, for example, up to 95% of reflectance obtained from plot-level reflectance may not come from the plant of interest, but rather from the soil (Dashti et al., 2019). Although dataset limitations made it unfeasible to comprehensively account for reflectance from confounding factors, NEON sampling protocols and the green vegetation indices analyzed (GLI and LAI; Appendix S1: Table S2) provide support that reflectance in our analysis represented the plant(s) of interest. Furthermore, high spectral resolution data can help overcome the influence of bare soil and more accurately capture vegetation dynamics compared with broadband vegetation indices in arid grasslands (Ren & Zhou, 2019). Lepine et al. (2016) found that spatial resolution was more important than spectral resolution for foliar N estimates in closed-canopy forested sites. Evaluation of plant traits across biomes with varying degrees of vegetation cover will likely benefit from data with high spatial and spectral resolutions. This type of data, however, is often costly, is geographically constrained, and can strain data storage and computational resources. Despite these limitations, advances in sensors, analytical techniques, and computational resources offer promise in the development of broadscale plant trait predictions that are generalizable across ecoregions to inform global-scale processes on the Earth's surface.

Broader applications and future work

Improved estimates of foliar N, especially regarding our PLSR results across and within biomes, will improve predictions of C dynamics in ESMs. Many ESMs use estimates of foliar N to predict an important photosynthetic parameter (maximum Rubisco activity, $V_{\rm c,max}$), which is then used to predict plant productivity and ultimately plant C uptake in terrestrial systems (Kattge et al., 2009; Rogers et al., 2017). Variations in C-sink predictions from these models are partially due to variability in foliar N estimates (Bonan et al., 2011; Friend, 2010). For example, Ghimire et al. (2016) showed a 70% reduction in GPP bias when root and foliar N traits acquired from a global plant

trait database were used in Community Land Model simulations. Unfortunately, however, these plant trait databases are built on time-consuming measurements and, as a result, have incomplete representation of species and geographic areas (Jetz et al., 2016). The improved foliar N estimates presented here could help fill these gaps and reduce uncertainty in ESMs.

Remote sensing data availability, a lack of large-scale ground sampling campaigns, and large processing requirements have made scaling predictions of plant traits to continental scales unfeasible in the past (Coops et al., 2003). Narrowband reflectance patterns across the EM spectrum were needed for high-quality foliar N predictions, but there has historically been a paucity of spaceborne hyperspectral instruments that provide consistent coverage of large areas of Earth's surface (Transon et al., 2018). Several forthcoming or recently launched hyperspectral missions, however, will present new opportunities such as the Hyperspectral Imager Suite (HISUI) Japanese mission, the Environmental Mapping and Analysis Program (EnMAP) German program, the PRecursore IperSpettrale della Missione Applicativa (PRIMSA) Italian mission, and NASA's Surface Biology and Geology (SBG) Designated Observable (Matsunaga et al., 2019; Transon et al., 2018). Ecological observatory networks similar to NEON are occurring across the globe-Australia's Terrestrial Ecosystem Research Network (TERN), the South African Environmental Research Observation Network (SAEON), the Chinese Ecological Research Network (CERN), the Critical Zone Exploration Network (CZEN), Long Term Ecological Observatory Networks in the United States (LTER), Long-Term Agroecosystem Research (LTAR), Europe (eLTER), Japan (JaLTER), Philippines (PhilTER), the Korean Ecological Observatory Network (KEON), and the global FLUXNET network—and will significantly improve our ability to predict fine-scale biogeochemical dynamics across the globe (Cleverly et al., 2019; Mirtl et al., 2018). As initiatives such as NEON progress, we will continue to improve plant trait predictions and our understanding of how variations in plant traits impact their light absorption and reflectance patterns under current and future conditions. These insights, in turn, can help inform and validate future satellite missions such as NASA's SBG and Earth Surface Mineral Dust Source Investigation (EMIT) to continue improvements in foliar N mapping across broad geographic areas. The results of this present analysis from divergent biomes across the United States, in combination with recent satellite, technological, and analytical advancements, support the development of robust continental-scale predictions of foliar N.

ACKNOWLEDGMENTS

This research was supported by NSF Award 1735693 (Doctoral Dissertation Research: Integrating Image

ECOSPHERE 15 of 18

Spectroscopy and Microbial Biogeochemistry to Analyze Woody Shrub Encroachment) and, in part, through synergistic work under NSF Award 1916896 (MSB-ECA: Leveraging NEON data to investigate remote sensing of biodiversity variables and scaling implications). Partial support was also provided by Arizona Agricultural Experiment Station AZRT-1390130-M12-222. Computing resources were provided by the Arizona Remote Sensing Center at the University of Arizona. We would also like to thank the anonymous reviewers whose comments helped improve this manuscript.

CONFLICT OF INTEREST

The authors declare no conflict of interest.

DATA AVAILABILITY STATEMENT

Plant foliar traits (NEON, 2021a; https://doi.org/10.48443/za0d-wn97), woody vegetation structure (NEON, 2021b; https://doi.org/10.48443/e3qn-xw47), high-resolution orthorectified camera imagery mosaic (NEON, 2021c; https://doi.org/10.48443/4e85-cr14), and spectrometer orthorectified surface directional reflectance–flight line data (NEON, 2021d; https://doi.org/10.48443/n3ys-2070) are all publicly available from the NEON data portal (https://www.neonscience.org/data). Subsequent data and code used in the analysis are available from Zenodo (Farella, 2021; https://doi.org/10.5281/zenodo.5542249).

ORCID

Martha M. Farella https://orcid.org/0000-0002-2925-4093

Mallory L. Barnes https://orcid.org/0000-0001-8528-6981

David D. Breshears https://orcid.org/0000-0001-6601-0058

Jessica Mitchell https://orcid.org/0000-0002-3126-010X Willem J. D. van Leeuwen https://orcid.org/0000-0002-3188-7172

Rachel E. Gallery https://orcid.org/0000-0002-9159-8778

REFERENCES

- Abdala-Roberts, L., S. Rasmann, J. C. Berny-Mier y Terán, F. Covelo, G. Glauser, and X. Moreira. 2016. "Biotic and Abiotic Factors Associated with Altitudinal Variation in Plant Traits and Herbivory in a Dominant Oak Species." *American Journal of Botany* 103: 2070–8.
- Ahlstrom, A., M. R. Raupach, G. Schurgers, B. Smith, A. Arneth, M. Jung, M. Reichstein, et al. 2015. "The Dominant Role of Semi-Arid Ecosystems in the Trend and Variability of the Land CO₂ Sink." *Science* 348: 895–9.
- Asner, G. P., R. E. Martin, C. B. Anderson, and D. E. Knapp. 2015. "Quantifying Forest Canopy Traits: Imaging Spectroscopy Versus Field Survey." *Remote Sensing of Environment* 158: 15–27.

- Bonan, G. B., P. J. Lawrence, K. W. Oleson, S. Levis, M. Jung, M. Reichstein, D. M. Lawrence, and S. C. Swenson. 2011. "Improving Canopy Processes in the Community Land Model Version 4 (CLM4) Using Global Flux Fields Empirically Inferred from FLUXNET Data." Journal of Geophysical Research 116: G02014.
- Carlson, T. N., and D. A. Ripley. 1997. "On the Relation between NDVI, Fractional Vegetation Cover, and Leaf Area Index." *Remote Sensing of Environment* 62: 241–52.
- Chadwick, K., and G. Asner. 2016. "Organismic-Scale Remote Sensing of Canopy Foliar Traits in Lowland Tropical Forests." Remote Sensing 8: 87.
- Chapin, F. S., P. A. Matson, and P. M. Vitousek. 2011. *Principles of Terrestrial Ecosystem Ecology*. New York: Springer.
- Chen, P., D. Haboudane, N. Tremblay, J. Wang, P. Vigneault, and B. Li. 2010. "New Spectral Indicator Assessing the Efficiency of Crop Nitrogen Treatment in Corn and Wheat." *Remote Sensing of Environment* 114: 1987–97.
- Chen, Y., W. Han, L. Tang, Z. Tang, and J. Fang. 2013. "Leaf Nitrogen and Phosphorus Concentrations of Woody Plants Differ in Responses to Climate, Soil and Plant Growth Form." *Ecography* 36: 178–84.
- Chlus, A., winstonolson, and E. Greenberg. 2019. "HyTools." https://github.com/EnSpec/hytools.
- Cho, M. A., and A. K. Skidmore. 2006. "A New Technique for Extracting the Red Edge Position from Hyperspectral Data: The Linear Extrapolation Method." *Remote Sensing of Environ*ment 101: 181–93.
- Cleverly, J., D. Eamus, W. Edwards, M. Grant, M. J. Grundy, A. Held, M. Karan, et al. 2019. "TERN, Australia's Land Observatory: Addressing the Global Challenge of Forecasting Ecosystem Responses to Climate Variability and Change." Environmental Research Letters 14: 095004.
- Clevers, J. G. P. W., and A. A. Gitelson. 2013. "Remote Estimation of Crop and Grass Chlorophyll and Nitrogen Content Using Red-Edge Bands on Sentinel-2 and -3." *International Journal of Applied Earth Observation and Geoinformation* 23: 344–51.
- Clevers, J. G. P. W., and L. Kooistra. 2012. "Using Hyperspectral Remote Sensing Data for Retrieving Canopy Chlorophyll and Nitrogen Content." *IEEE Journal of Selected Topics in Applied Earth Observations and Remote Sensing* 5: 574–83.
- Colgan, M., C. Baldeck, J.-B. Féret, and G. Asner. 2012. "Mapping Savanna Tree Species at Ecosystem Scales Using Support Vector Machine Classification and BRDF Correction on Airborne Hyperspectral and LiDAR Data." Remote Sensing 4: 3462–80.
- Coops, N. C., M.-L. Smith, M. E. Martin, and S. V. Ollinger. 2003. "Prediction of Eucalypt Foliage Nitrogen Content from Satellite-Derived Hyperspectral Data." *IEEE Transactions on Geoscience and Remote Sensing* 41: 1338–46.
- Curran, P. J. 1989. "Remote Sensing of Foliar Chemistry." *Remote Sensing of Environment* 30: 271–8.
- Dashti, H., N. F. Glenn, S. Ustin, J. J. Mitchell, Y. Qi, N. T. Ilangakoon, A. N. Flores, et al. 2019. "Empirical Methods for Remote Sensing of Nitrogen in Drylands May Lead to Unreliable Interpretation of Ecosystem Function." IEEE Transactions on Geoscience and Remote Sensing 57: 3993–4004.
- Dumas, J. B. A. 1831. "Procedes de l'analyse Organic." *Annals of Chemistry and of Physics* 247: 198–213.
- Eisfelder, C., C. Kuenzer, and S. Dech. 2012. "Derivation of Biomass Information for Semi-Arid Areas Using Remote-Sensing Data." *International Journal of Remote Sensing* 33: 2937–84.

Elvidge, C. D. 1990. "Visible and near Infrared Reflectance Characteristics of Dry Plant Materials." *International Journal of Remote Sensing* 11: 1775–95.

- Evans, J. R., and V. C. Clarke. 2019. "The Nitrogen Cost of Photosynthesis." *Journal of Experimental Botany* 70: 7–15.
- Farella, M. 2021. "marthageb/FoliarN_NEON: Code and Data for Ecosphere." Zenodo. https://doi.org/10.5281/zenodo.5542249.
- Feilhauer, H., G. P. Asner, R. E. Martin, and S. Schmidtlein. 2010. "Brightness-Normalized Partial Least Squares Regression for Hyperspectral Data." *Journal of Quantitative Spectroscopy and Radiative Transfer* 111: 1947–57.
- Field, C., and H. A. Mooney. 1986. "The Photosynthesis-Nitrogen Relationship in Wild Plants." In On the Economy of Plant Form and Function, edited by T.J. Givnish, 25–55. Cambridge: Cambridge University Press.
- Field, C. B. 1998. "Primary Production of the Biosphere: Integrating Terrestrial and Oceanic Components." *Science* 281: 237–40.
- Franks, P. J., G. B. Bonan, J. A. Berry, D. L. Lombardozzi, N. M. Holbrook, N. Herold, and K. W. Oleson. 2018. "Comparing Optimal and Empirical Stomatal Conductance Models for Application in Earth System Models." *Global Change Biology* 24: 5708–23.
- Friend, A. D. 2010. "Terrestrial Plant Production and Climate Change." *Journal of Experimental Botany* 61: 1293–309.
- Gamon, J. A., B. Somers, Z. Malenovský, E. M. Middleton, U. Rascher, and M. E. Schaepman. 2019. "Assessing Vegetation Function with Imaging Spectroscopy." Surveys in Geophysics 40: 489–513.
- Gastal, F., and B. Saugier. 1989. "Relationships between Nitrogen Uptake and Carbon Assimilation in Whole Plants of Tall Fescue." Plant, Cell and Environment 12: 407–18.
- Ghimire, B., W. J. Riley, C. D. Koven, M. Mu, and J. T. Randerson. 2016. "Representing Leaf and Root Physiological Traits in CLM Improves Global Carbon and Nitrogen Cycling Predictions: Leaf and Root Traits in CLM." Journal of Advances in Modeling Earth Systems 8: 598–613.
- Glenn, E., A. Huete, P. Nagler, and S. Nelson. 2008. "Relationship between Remotely-Sensed Vegetation Indices, Canopy Attributes and Plant Physiological Processes: What Vegetation Indices Can and Cannot Tell Us about the Landscape." Sensors 8: 2136–60.
- Goll, D. S., V. Brovkin, B. R. Parida, C. H. Reick, J. Kattge, P. B. Reich, P. M. van Bodegom, and Ü. Niinemets. 2012. "Nutrient Limitation Reduces Land Carbon Uptake in Simulations with a Model of Combined Carbon, Nitrogen and Phosphorus Cycling." *Biogeosciences* 9: 3547–69.
- Green, R. O., M. L. Eastwood, C. M. Sarture, T. G. Chrien, M. Aronsson, B. J. Chippendale, J. A. Faust, et al. 1998. "Imaging Spectroscopy and the Airborne Visible/Infrared Imaging Spectrometer (AVIRIS)." *Remote Sensing of Environment* 65: 227–48.
- Hilker, T. 2018. "Surface Reflectance/Bidirectional Reflectance Distribution Function." In Liang, S., *Comprehensive Remote Sensing*. 2–8. Cham: Elsevier.
- Horneck, D. A., and R. O. Miller. 1997. "Determination of Total Nitrogen in Plant Tissue." In *Handbook of Reference Methods* for Plant Analysis. 75–84. Boca Raton, FL: CRC Press.
- Hu, T., and R. Smith. 2018. "The Impact of Hurricane Maria on the Vegetation of Dominica and Puerto Rico Using Multispectral Remote Sensing." *Remote Sensing* 10: 827.

Huete, A. R. 1988. "A Soil-Adjusted Vegetation Index (SAVI)." Remote Sensing of Environment 25: 295–309.

- Hulslander, D. 2019. NEON Algorithm Theoretical Basis Document (ATBD): Leaf Area Index, Vol 01. Boulder, CO: NEON.
- Jetz, W., J. Cavender-Bares, R. Pavlick, D. Schimel, F. W. Davis, G. P. Asner, R. Guralnick, et al. 2016. "Monitoring Plant Functional Diversity from Space." *Nature Plants* 2: 16024.
- Johnson, B. R., T. U. Kampe, and M. Kuester. 2010. "Development of Airborne Remote Sensing Instrumentations for NEON", In Proc. SPIE 7809, Remote Sensing and Modeling of Ecosystems for Sustainability VII, 78090I (12 August 2010); https://doi.org/ 10.1117/12.860182
- Kalacska, M., M. Lalonde, and T. R. Moore. 2015. "Estimation of Foliar Chlorophyll and Nitrogen Content in an Ombrotrophic Bog from Hyperspectral Data: Scaling from Leaf to Image." Remote Sensing of Environment 169: 270–9.
- Kampe, T. U. 2010. "NEON: The First Continental-Scale Ecological Observatory with Airborne Remote Sensing of Vegetation Canopy Biochemistry and Structure." *Journal of Applied Remote Sensing* 4: 043510.
- Kattge, J., W. Knorr, T. Raddatz, and C. Wirth. 2009. "Quantifying Photosynthetic Capacity and Its Relationship to Leaf Nitrogen Content for Global-Scale Terrestrial Biosphere Models." *Global Change Biology* 15: 976–91.
- Kjeldahl, J. 1883. "Neue Methode zur Bestimmung des Stickstoffs in organischen Körpern." Fresenius' Zeitschrift für Analytische Chemie 22: 366–82.
- Knyazikhin, Y., M. A. Schull, P. Stenberg, M. Mottus, M. Rautiainen, Y. Yang, A. Marshak, et al. 2013. "Hyperspectral Remote Sensing of Foliar Nitrogen Content." *Proceedings of the National Academy of Sciences* 110: E185–92.
- Köppen, W. 2011. "The Thermal Zones of the Earth According to the Duration of Hot, Moderate and Cold Periods and to the Impact of Heat on the Organic World." *Meteorologische Zeitschrift* 20: 351–60.
- Kottek, M., J. Grieser, C. Beck, B. Rudolf, and F. Rubel. 2006. "World Map of the Köppen-Geiger Climate Classification Updated." *Meteorologische Zeitschrift* 15: 259–63.
- Lepine, L. C., S. V. Ollinger, A. P. Ouimette, and M. E. Martin. 2016. "Examining Spectral Reflectance Features Related to Foliar Nitrogen in Forests: Implications for Broad-Scale Nitrogen Mapping." *Remote Sensing of Environment* 173: 174–86.
- Li, X., and A. H. Strahler. 1992. "Geometric-Optical Bidirectional Reflectance Modeling of the Discrete Crown Vegetation Canopy: Effect of Crown Shape and Mutual Shadowing." *IEEE Transactions on Geoscience and Remote Sensing* 30: 276–92.
- Liang, S., X. Li, and J. Wang. 2012. Advanced Remote Sensing: Terrestrial Information Extraction and Applications. Amsterdam: Academic Press.
- Los, S. O., P. R. J. North, W. M. F. Grey, and M. J. Barnsley. 2005. "A Method to Convert AVHRR Normalized Difference Vegetation Index Time Series to a Standard Viewing and Illumination Geometry." *Remote Sensing of Environment* 99: 400–11.
- Louhaichi, M., M. M. Borman, and D. E. Johnson. 2001. "Spatially Located Platform and Aerial Photography for Documentation of Grazing Impacts on Wheat." *Geocarto International* 16: 65–70.
- Lunch, C., C. Laney, N. Mietkiewicz, E. Sokol, K. Cawley & NEON (National Ecological Observatory Network). 2021.

ECOSPHERE 17 of 18

neonUtilities: Utilities for Working with NEON Data. https://CRAN.R-project.org/package=neonUtilities

- Mahlstein, I., J. S. Daniel, and S. Solomon. 2013. "Pace of Shifts in Climate Regions Increases with Global Temperature." *Nature Climate Change* 3: 739–43.
- Martin, M. E., L. C. Plourde, S. V. Ollinger, M.-L. Smith, and B. E. McNeil. 2008. "A Generalizable Method for Remote Sensing of Canopy Nitrogen across a Wide Range of Forest Ecosystems." Remote Sensing of Environment 112: 3511–9.
- Matsunaga, T., K. Obata, K. Mouri, T. Tachikawa, A. Iwasaki, S. Tsuchida, K. Iwao, et al. 2019. "HISUI Status Toward 2020 Launch." In IGARSS 2019–2019 IEEE International Geoscience and Remote Sensing Symposium. 4495–8. Yokohama: IEEE.
- Mehmood, T., K. H. Liland, L. Snipen, and S. Sæbø. 2012. "A Review of Variable Selection Methods in Partial Least Squares Regression." Chemometrics and Intelligent Laboratory Systems 118: 62–9.
- Mevik, B.-H., R. Wehrens & K. H. Liland 2020. pls: Partial Least Squares and Principal Component Regression. https://CRAN. R-project.org/package=pls
- Millennium Ecosystem Assessment. 2005. Ecosystems and Human Well-Being. Washington, DC: Island Press.
- Mirtl, M., E. T. Borer, I. Djukic, M. Forsius, H. Haubold, W. Hugo, J. Jourdan, et al. 2018. "Genesis, Goals and Achievements of Long-Term Ecological Research at the Global Scale: A Critical Review of ILTER and Future Directions." Science of the Total Environment 626: 1439–62.
- Mutanga, O., and A. K. Skidmore. 2007. "Red Edge Shift and Biochemical Content in Grass Canopies." ISPRS Journal of Photogrammetry and Remote Sensing 62: 34–42.
- NEON. 2020. geoNEON: Geolocation Data Access for NEON Data. Boulder, CO: NEON.
- NEON. 2021a. Plant Foliar Traits (DP1.10026.001): Release-2021. Boulder, CO: NEON.
- NEON. 2021b. Woody Plant Vegetation Structure (DP1.10098.001): Release-2021. Boulder, CO: NEON.
- NEON. 2021c. High-Resolution Orthorectified Camera Imagery Mosaic (DP3.30010.001): Release-2021. Boulder, CO: NEON.
- NEON. 2021d. Spectrometer Orthorectified Surface Directional Reflectance—Flightline (DP1.30006.001): Release-2021. Boulder, CO: NEON.
- Ollinger, S. V. 2011. "Sources of Variability in Canopy Reflectance and the Convergent Properties of Plants." *New Phytologist* 189: 375–94.
- Ollinger, S. V., A. D. Richardson, M. E. Martin, D. Y. Hollinger, S. E. Frolking, P. B. Reich, L. C. Plourde, et al. 2008. "Canopy Nitrogen, Carbon Assimilation, and Albedo in Temperate and Boreal Forests: Functional Relations and Potential Climate Feedbacks." Proceedings of the National Academy of Sciences 105: 19336–41.
- Ollinger, S. V., and M.-L. Smith. 2005. "Net Primary Production and Canopy Nitrogen in a Temperate Forest Landscape: An Analysis Using Imaging Spectroscopy, Modeling and Field Data." *Ecosystems* 8: 760–78.
- Osnas, J. L. D., M. Katabuchi, K. Kitajima, S. J. Wright, P. B. Reich, S. A. Van Bael, N. J. B. Kraft, M. J. Samaniego, S. W. Pacala, and J. W. Lichstein. 2018. "Divergent Drivers of Leaf Trait Variation within Species, among Species, and among Functional Groups." Proceedings of the National Academy of Sciences 115: 5480–5.

- Poulter, B., P. Ciais, E. Hodson, H. Lischke, F. Maignan, S. Plummer, and N. E. Zimmermann. 2011. "Plant Functional Type Mapping for Earth System Models." *Geoscientific Model Development* 4: 993–1010.
- Poulter, B., D. Frank, P. Ciais, R. B. Myneni, N. Andela, J. Bi, G. Broquet, et al. 2014. "Contribution of Semi-Arid Ecosystems to Interannual Variability of the Global Carbon Cycle." *Nature* 509: 600–3.
- R Core Team. 2021. R: A Language and Environment for Statistical Computing. Vienna: R Foundation for Statistical Computing.
- Ramoelo, A., A. K. Skidmore, M. A. Cho, M. Schlerf, R. Mathieu, and I. M. A. Heitkönig. 2012. "Regional Estimation of Savanna Grass Nitrogen Using the Red-Edge Band of the Spaceborne RapidEye Sensor." International Journal of Applied Earth Observation and Geoinformation 19: 151–62.
- Ren, H., and G. Zhou. 2019. "Estimating Green Biomass Ratio with Remote Sensing in Arid Grasslands." *Ecological Indicators* 98: 568–74.
- Reyniers, M., D. J. J. Walvoort, and J. De Baardemaaker. 2006. "A Linear Model to Predict with a Multi-Spectral Radiometer the Amount of Nitrogen in Winter Wheat." *International Journal of Remote Sensing* 27: 4159–79.
- Rogers, A. 2014. "The Use and Misuse of $V_{c,max}$ in Earth System Models." *Photosynthesis Research* 119: 15–29.
- Rogers, A., B. E. Medlyn, J. S. Dukes, G. Bonan, S. Caemmerer, M. C. Dietze, J. Kattge, et al. 2017. "A Roadmap for Improving the Representation of Photosynthesis in Earth System Models." *New Phytologist* 213: 22–42.
- Ross, J. 1981. The Radiation Regime and Architecture of Plant Stands. Berlin: Springer Science & Business Media.
- Rubel, F., K. Brugger, K. Haslinger, and I. Auer. 2017. "The Climate of the European Alps: Shift of Very High Resolution Köppen-Geiger Climate Zones 1800–2100." Meteorologische Zeitschrift 26: 115–25.
- Schaaf, C. B., F. Gao, A. H. Strahler, W. Lucht, X. Li, T. Tsang, N. C. Strugnell, et al. 2002. "First Operational BRDF, Albedo Nadir Reflectance Products from MODIS." Remote Sensing of Environment 83: 135–48.
- Schmidt, H., and A. Karnieli. 2000. "Remote Sensing of the Seasonal Variability of Vegetation in a Semi-Arid Environment." *Journal of Arid Environments* 45: 43–59.
- Serbin, S. P., and P. A. Townsend. 2020. "Scaling Functional Traits from Leaves to Canopies." In *Remote Sensing of Plant Biodiversity*, edited by J. Cavender-Bares, J.A. Gamon, and P.A. Townsend, 43–82. Cham: Springer International Publishing.
- Serrano, L., J. Peñuelas, and S. L. Ustin. 2002. "Remote Sensing of Nitrogen and Lignin in Mediterranean Vegetation from AVIRIS Data." Remote Sensing of Environment 81: 355–64.
- Sims, D. A., and J. A. Gamon. 2003. "Estimation of Vegetation Water Content and Photosynthetic Tissue Area from Spectral Reflectance: A Comparison of Indices Based on Liquid Water and Chlorophyll Absorption Features." *Remote Sensing of Environment* 84: 526–37.
- Singh, A., S. P. Serbin, B. E. McNeil, C. C. Kingdon, and P. A. Townsend. 2015. "Imaging Spectroscopy Algorithms for Mapping Canopy Foliar Chemical and Morphological Traits and Their Uncertainties." *Ecological Applications* 25: 2180–97.
- Skidmore, A. K., J. G. Ferwerda, O. Mutanga, S. E. Van Wieren, M. Peel, R. C. Grant, H. H. T. Prins, F. B. Balcik, and V. Venus.

2010. "Forage Quality of Savannas—Simultaneously Mapping Foliar Protein and Polyphenols for Trees and Grass Using Hyperspectral Imagery." *Remote Sensing of Environment* 114: 64–72.

- Smith, M.-L., M. E. Martin, L. Plourde, and S. V. Ollinger. 2003. "Analysis of Hyperspectral Data for Estimation of Temperate Forest Canopy Nitrogen Concentration: Comparison between an Airborne (Aviris) and a Spaceborne (Hyperion) Sensor." *IEEE Transactions on Geoscience and Remote Sensing* 41: 1332–7.
- Smith, W. K., M. P. Dannenberg, D. Yan, S. Herrmann, M. L. Barnes, G. A. Barron-Gafford, J. A. Biederman, et al. 2019. "Remote Sensing of Dryland Ecosystem Structure and Function: Progress, Challenges, and Opportunities." *Remote Sensing of Environment* 233: 111401.
- Soenen, S. A., D. R. Peddle, and C. A. Coburn. 2005. "SCS+C: A Modified Sun-Canopy-Sensor Topographic Correction in Forested Terrain." *IEEE Transactions on Geoscience and Remote* Sensing 43: 2148–59.
- Tian, Y. C., J. Yang, X. Yao, Y. Zhu, and W. X. Cao. 2010. "A Newly Developed Blue Nitrogen Index for Estimating Canopy Leaf Nitrogen Concentration of Rice." *Chinese Journal of Applied Ecology* 21: 966–72.
- Transon, J., R. d'Andrimont, A. Maugnard, and P. Defourny. 2018. "Survey of Hyperspectral Earth Observation Applications from Space in the Sentinel-2 Context." *Remote Sensing* 10: 157.
- UNEP-WCMC. 2011. Global Drylands: A UN System-Wide Response. Geneva: United Nations Environmental Management Group.
- Ustin, S. L., and S. Jacquemoud. 2020. "How the Optical Properties of Leaves Modify the Absorption and Scattering of Energy and Enhance Leaf Functionality." In *Remote Sensing of Plant Biodiversity*, edited by J. Cavender-Bares, J.A. Gamon, and P.A. Townsend, 349–84. Cham: Springer International Publishing.
- van Deventer, H., M. A. Cho, O. Mutanga, and A. Ramoelo. 2015. "Capability of Models to Predict Leaf N and P across Four Seasons for Six Sub-Tropical Forest Evergreen Trees." ISPRS Journal of Photogrammetry and Remote Sensing 101: 209–20.
- Vicente-Serrano, S. M. 2007. "Evaluating the Impact of Drought Using Remote Sensing in a Mediterranean, Semi-Arid Region." *Natural Hazards* 40: 173–208.
- Wang, W., X. Yao, Y. Tian, X. Liu, J. Ni, W. Cao, and Y. Zhu. 2012.
 "Common Spectral Bands and Optimum Vegetation Indices for Monitoring Leaf Nitrogen Accumulation in Rice and Wheat." *Journal of Integrative Agriculture* 11: 2001–12.
- Wang, W., X. Yao, X. Yao, Y. Tian, X. Liu, J. Ni, W. Cao, and Y. Zhu. 2012. "Estimating Leaf Nitrogen Concentration with Three-Band Vegetation Indices in Rice and Wheat." Field Crops Research 129: 90–8.
- Wang, Y.-P., and B. Z. Houlton. 2009. "Nitrogen Constraints on Terrestrial Carbon Uptake: Implications for the Global Carbon-Climate Feedback." *Geophysical Research Letters* 36: L24403.

- Wang, Z., A. Chlus, R. Geygan, Z. Ye, T. Zheng, A. Singh, J. J. Couture, J. Cavender-Bares, E. L. Kruger, and P. A. Townsend. 2020. "Foliar Functional Traits from Imaging Spectroscopy across Biomes in Eastern North America." New Phytologist 228: 494–511.
- Wang, Z., T. Wang, R. Darvishzadeh, A. Skidmore, S. Jones, L. Suarez, W. Woodgate, U. Heiden, M. Heurich, and J. Hearne. 2016. "Vegetation Indices for Mapping Canopy Foliar Nitrogen in a Mixed Temperate Forest." *Remote Sensing* 8: 491.
- Wanner, W., X. Li, and A. H. Strahler. 1995. "On the Derivation of Kernels for Kernel-Driven Models of Bidirectional Reflectance." *Journal of Geophysical Research* 100: 21077.
- Wårlind, D., B. Smith, T. Hickler, and A. Arneth. 2014. "Nitrogen Feedbacks Increase Future Terrestrial Ecosystem Carbon Uptake in an Individual-Based Dynamic Vegetation Model." *Biogeosciences* 11: 6131–46.
- Warnes, G. R., B. Bolker, L. Bonebakker, R. Gentleman, W. Huber, A. Liaw, T. Lumley, et al. 2020. gplots: Various R Programming Tools for Plotting Data. https://CRAN.R-project.org/package=gplots
- Weintraub, S., and E. Hinckley. 2017. TOS Protocol and Procedure: CFC—Canopy Foliage Sampling. Boulder, CO: NEON.
- Weyermann, J., M. Kneubuhler, D. Schlapfer, and M. E. Schaepman. 2015. "Minimizing Reflectance Anisotropy Effects in Airborne Spectroscopy Data Using Ross–Li Model Inversion with Continuous Field Land Cover Stratification." *IEEE Transactions on Geoscience and Remote Sensing* 53: 5814–23.
- Xue, L., W. Cao, W. Luo, T. Dai, and Y. Zhu. 2004. "Monitoring Leaf Nitrogen Status in Rice with Canopy Spectral Reflectance." Agronomy Journal 96: 135.
- Zhu, Y., X. Yao, Y. Tian, X. Liu, and W. Cao. 2008. "Analysis of Common Canopy Vegetation Indices for Indicating Leaf Nitrogen Accumulations in Wheat and Rice." *International Journal* of Applied Earth Observation and Geoinformation 10: 1–10.

SUPPORTING INFORMATION

Additional supporting information may be found in the online version of the article at the publisher's website.

How to cite this article: Farella, Martha M., Mallory L. Barnes, David D. Breshears, Jessica Mitchell, Willem J. D. van Leeuwen, and Rachel E. Gallery. 2022. "Evaluation of Vegetation Indices and Imaging Spectroscopy to Estimate Foliar Nitrogen across Disparate Biomes." *Ecosphere* 13(3): e3992. https://doi.org/10.1002/ecs2.3992